

# Resonance and scattering in microstructured optical fibers

T. P. White, R. C. McPhedran, and C. Martijn de Sterke

*School of Physics, University of Sydney, Sydney, NSW 2006, Australia*

N. M. Litchinitser and B. J. Eggleton

*OFS Laboratories, 19 Schoolhouse Road, Somerset, New Jersey 08873*

Received June 27, 2002

We present an investigation into the mechanism for guidance of microstructured optical fibers consisting of high-refractive-index cylinders embedded in a low-index background. A new guidance regime is identified in which the fibers' confinement losses depend strongly on wavelength and the positions of the loss minima and maxima depend on the scattering properties of individual cylinders and only weakly on their position and number. We point out similarities between these results and those reported recently for two-dimensional antiresonant reflecting waveguides. © 2002 Optical Society of America

OCIS codes: 060.2400, 060.2270, 230.3990, 290.1350.

Microstructured optical fibers (MOFs) consisting of air holes extending down the length of a silica optical fiber have been the subject of much interest in recent years because of their unusual dispersive and guidance properties (see, for example, Refs. 1 and 2). Two distinct types of guidance have been described: effective index guidance and bandgap guidance. Fibers that exhibit the first type typically have a core region of higher refractive index than the cylinders and are guided by a mechanism somewhat similar to that in conventional step-index fibers. Bandgap guiding is more subtle; it arises from coherent Bragg scattering from the periodic arrangement of cylinders surrounding the core region, which may be a larger air hole or a material of lower refractive index than the surrounding medium. Fibers of this type that are able to guide light in a large air core have potentially exciting applications in low-loss and high-power laser transmission. Bandgap guidance in fibers is not limited to MOFs with low-index cylinders nor only to MOF-type structures. Similar properties were recently reported in fibers with high-index cylinders embedded in silica,<sup>3</sup> and other fibers formed by multiple rings of high- and low-index dielectrics have also been shown to exhibit bandgap guiding.<sup>4</sup>

Some of the present authors recently reported the results of a theoretical study of the guidance mechanisms of antiresonant reflecting optical waveguides.<sup>5</sup> A new guiding regime was identified in such waveguides whose spectral properties are governed largely by the thickness and the refractive-index contrast of the first high-index layer rather than by the periodicity of the alternating layers. It was shown that this effect is dominant in the short-wavelength region, whereas Bragg reflection from the multiple layers becomes more important at longer wavelengths. It was proposed<sup>5</sup> that a similar effect may be present in MOFs composed of rings of high-index cylinders embedded in a lower-index background.<sup>3</sup>

In the layered structures referred to in the previous paragraph the modal properties depend on the first layer in the cladding and do not depend strongly on the

period. Here we extend this idea a step further and consider the properties of several MOF structures with cylinders of refractive index  $n_{\text{cyl}} = 1.8$  embedded in silica, which is taken to have a fixed index of  $n_e = 1.44$ . Using a rigorous full vector multipole method,<sup>6,7</sup> we can calculate accurately the modal properties of any finite arrangement of nonoverlapping cylindrical inclusions in a homogeneous background. In particular, the modal confinement loss can be obtained from complex propagation constant  $\beta$ , the imaginary part of which describes the modal attenuation along the fiber.

Our calculations show that even a single ring of cylinders has modes that are centered in the core region, as shown in Fig. 1 for a regular hexagonal structure with six cylinders of diameter  $3.315 \mu\text{m}$  spaced by  $\Lambda = 5.64 \mu\text{m}$ . The field profile of this fundamental mode is similar to those of index-guiding MOFs with air holes. The mode's effective index is  $n_{\text{eff}} = 1.4383661 + i7.878 \times 10^{-6}$  at  $\lambda = 0.792 \mu\text{m}$ . The imaginary part of  $n_{\text{eff}}$  is proportional to the confinement loss, which here is 540 dB/m. Note that  $n_{\text{eff}} < n_e < n_{\text{cyl}}$ ; thus the effective index is outside the range of bound modes in the individual cylinders. The loss decreases as more rings are added

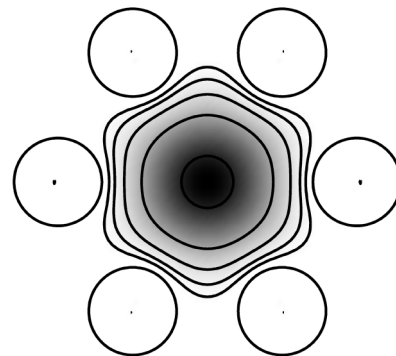


Fig. 1. Longitudinal Poynting vector,  $S_z = \frac{1}{2} \text{Re}(\mathbf{E} \times \mathbf{H}^*)z$ , of the fundamental mode of a regular six-cylinder MOF at  $\lambda = 0.792 \mu\text{m}$ . Cylinder diameter,  $3.315 \mu\text{m}$ ; refractive index,  $n_{\text{cyl}} = 1.8$ ; cylinder spacing,  $5.64 \mu\text{m}$ ; background refractive index,  $n_e = 1.44$ .

to the structure, improving by more than 4 orders of magnitude when two extra rings are added. The fundamental mode of the MOF structure was calculated over a range of wavelengths from 0.6 to 1.25  $\mu\text{m}$ , and the real and imaginary parts of the effective index are shown in Fig. 2 [curves (1)]. The loss spectrum of the mode is quite complicated, consisting of a number of lower-loss regions separated by narrow regions where the loss rapidly increases. Several other narrow features can be seen at other wavelengths. This behavior is fundamentally different from that displayed by index-guiding MOF structures, for which the loss increases monotonically with wavelength.<sup>8</sup> The real part of  $n_{\text{eff}}$  also changes rapidly in the same regions, a result consistent with the Kramers–Kronig relations. Curves (2) show the results for the same structure but with three rings of holes. The real part of  $n_{\text{eff}}$  is almost unchanged, but the losses are significantly decreased. However, the wavelengths at which the loss is maximum are unchanged by the addition of more rings.

The remaining curves in Fig. 2 show the real and imaginary parts of the modal effective index for several other MOFs with cylinders identical to the first ones but in different numbers and arrangements. Curves (3) and (4) correspond to a structure with a circular ring of 10 cylinders (Fig. 2, inset diagrams), spaced by 5.03 and 7.09  $\mu\text{m}$ , respectively, and curves (5) are for a higher-order mode of the randomized 10-cylinder structure shown in the inset. Not all the curves have been calculated over the full wavelength range, but it is still clear that, whereas the actual values of the effective index differ for each structure, the loss curves are all similar in shape and the high-loss regions occur near the same wavelengths for all structures. This result is surprising and raises a number of interesting issues. As the only parameters that are unchanged among all the structures are the cylinder size and refractive index, it is natural to investigate the properties of an individual cylinder to understand the behavior of the multicylinder structures.

The scattering properties of dielectric cylinders are well understood, and a number of vector treatments have been formulated. We follow the treatment in Refs. 9 and 10 for the scattering of a plane wave with oblique incidence upon an infinite dielectric cylinder. We can represent the fields of the incident wave propagating in the  $x$ - $z$  plane, at an angle of  $\pi/2 - \alpha$  relative to the cylinder ( $z$  axis), as a series of  $J$ -type Bessel functions by using the expansion

$$\exp(ilx + ihz - i\omega t) = \exp(ihz - i\omega t) \times \sum_{n=-\infty}^{\infty} J_n(lr) \exp(in\theta), \quad (1)$$

where  $k = n_e \omega / c$ ,  $l = k \cos(\alpha)$ , and  $h = k \sin(\alpha)$ . The scattered fields are expressed in terms of Hankel  $H_n^{(1)}(lr)$  functions centered on the cylinder, and the fields inside the cylinder are expressed as a  $J$ -type Bessel function series with argument  $rl_1$ , where  $l_1 = (n_{\text{cyl}}^2 k^2 - h^2)^{1/2}$  is the transverse wave number inside the cylinder. The boundary conditions that

require continuity of  $E_z$ ,  $E_\phi$ ,  $H_z$ , and  $H_\phi$  are applied analytically on the surface of the cylinder to produce expressions for the expansion coefficients, allowing all the field components to be calculated. The plane-wave scattering results that we present below are all for  $E$  polarization, where the incident electric field lies in the  $x$ - $z$  plane. We have performed the same calculations for the  $H$ -polarization case with little change in the essential behavior.

In Fig. 3 we compare the loss profile of the six-cylinder MOF from Fig. 2 [shown in Fig. 3(a)] with two properties of the plane-wave scattering from a single cylinder. The angle of incidence of the plane wave must be specified in the calculations, so  $\alpha$  was varied according to the effective index of the MOF mode at each wavelength. However, we found that these effective index variations over the range shown in Fig. 2(a) result only in minor changes to the overall behavior. Thus, even though each of the MOF geometries investigated has modes of different  $n_{\text{eff}}$ , the loss properties are all similar. Figure 3(b) shows the total scattering cross section of a single cylinder as a function of wavelength over the range  $0.758 \mu\text{m} < \lambda < 1.095 \mu\text{m}$ , covering four successive high-loss peaks of the MOF modes. Observe that the scattering resonances correspond to large losses, suggesting that the scattering properties of a single cylinder are driving the guidance properties of the MOF. We can best understand the driving role of

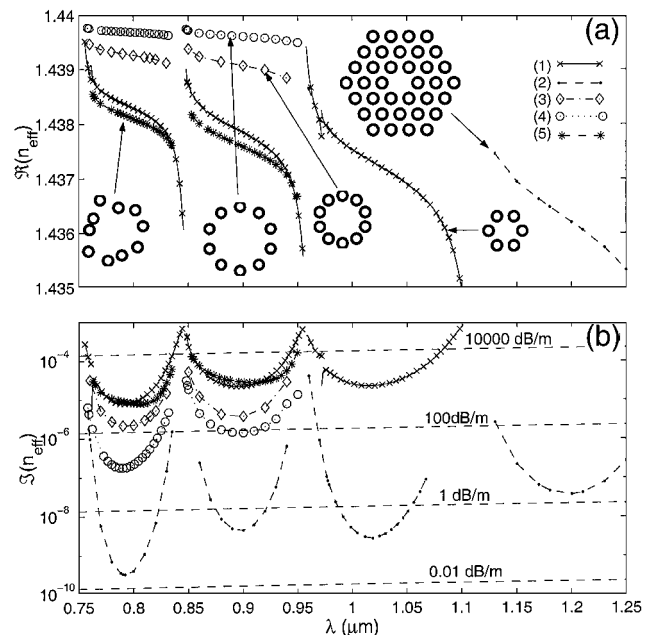


Fig. 2. (a) Real and (b) imaginary parts of the effective index of MOF modes for a number of different geometries. Curves (1), single hexagonal ring with  $\Lambda = 5.64 \mu\text{m}$ ; curves (2), three-ring hexagonal structure with  $\Lambda = 5.64 \mu\text{m}$ ; curves (3), 10-cylinder ring structure with  $\Lambda = 5.03 \mu\text{m}$ ; curves (4), 10-cylinder ring structure with  $\Lambda = 7.09 \mu\text{m}$ ; curves (5), random arrangement of 10 cylinders around the core region. Inset diagrams, the respective hole arrangements. The four dashed lines in (b) are contours of constant confinement loss in decibels per meter.

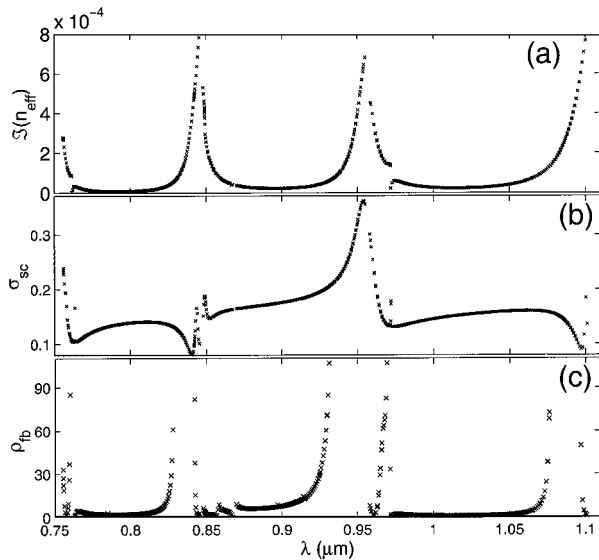


Fig. 3. Comparison of MOF loss characteristics with the plane-wave scattering properties of a single cylinder. (a) Imaginary part of the effective index of the six-cylinder MOF shown in Fig. 2. (b) Scattering cross section of a single cylinder (arbitrary units). (c) Forward-to-backward scattering ratio, as defined in Eq. (2).

the single-cylinder scattering by considering the direction as well as the magnitude of the scattering. Figure 3(c) shows the ratio of forward to backward scattering from the cylinder, which we define in terms of radial Poynting vector  $S_r$  of the total field (incident plus scattered) as

$$\rho_{fb} = \frac{\int^{\text{forward}} \delta_{\text{out}}(r_c, \phi) S_r(r_{\text{cyl}}, \phi) d\phi}{\int^{\text{backward}} \delta_{\text{out}}(r_c, \phi) S_r(r_{\text{cyl}}, \phi) d\phi}, \quad (2)$$

where the integrals are calculated about the forward- and backward-facing halves of the cylinder boundary, defined by the direction of the incident wave, and  $\delta_{\text{out}}(r_c, \phi) = 0$  if  $S_r < 0$  and  $\delta_{\text{out}}(r_c, \phi) = 1$  if  $S_r > 0$ . This is a measure of the ratio of energy flowing out of the cylinder in the forward ( $x > 0$ ) direction to the energy that is being reflected back in the  $x < 0$  direction. Comparing the MOF loss curve with the forward-to-backward scattering ratio, we can see that there is good qualitative agreement between the two results. Note that some of the smaller details of the loss spectrum are also predicted accurately by the scattering ratio for the single cylinder. For example, at  $\lambda = 0.972 \mu\text{m}$  the confinement loss of the MOF exhibits a sharp decrease, as shown in Fig. 3(a), corresponding to the narrow scattering resonance seen in Fig. 3(b) and to a similar decrease in  $\rho_{fb}$ .

In conclusion, we have shown that the modal loss characteristics of MOFs with high-index cylinders surrounding a low-index core region can be understood in terms of the scattering of a plane wave from a single cylinder. When the forward scattering peaks, light can easily leak from the core through the cylinders, resulting in high losses. Confinement is best when the forward scattering is minimized relative to the backward scattering. In this respect there is a clear analogy between the resonant tunneling leakage mechanism of the antiresonant reflecting optical waveguides in Ref. 5 and the forward-scattering leakage identified here. In MOFs in which this type of confinement dominates, the positioning of the cylinders about the core region has little effect on the overall loss characteristics, changing only the actual value of the loss and the effective index of the guided modes. This study also suggests that, if the high-index cylinders are used as elements in a bandgap guiding MOF, the bandgap is likely to be enhanced when the Bragg condition coincides with maximum backscattering from the cylinders. It is not clear whether guidance by low-index cylinders can also be explained by study of single-cylinder scattering and this will be a topic for future research.

T. P. White's e-mail address is [twhite@physics.usyd.edu.au](mailto:twhite@physics.usyd.edu.au).

## References

1. J. C. Knight, T. A. Birks, P. St. J. Russell, and D. M. Atkin, *Opt. Lett.* **25**, 25 (1996).
2. J. H. Eberly, *Opt. Express* **9**, 674 (2001), [www.opticsexpress.org](http://www.opticsexpress.org).
3. R. T. Bise, R. S. Windeler, K. S. Kranz, C. Kerbage, B. J. Eggleton, and D. J. Trevor, in *Optical Fiber Communication Conference*, Postconference Edition, Vol. 70 of OSA Trends in Optics and Photonics Series (Optical Society of America, Washington, D.C., 2002), pp. 466–468.
4. M. Ibanescu, Y. Fink, S. Fan, E. L. Thomas, and J. D. Joannopoulos, *Science* **289**, 1537 (1999).
5. N. M. Litchinitser, A. K. Abeeluck, C. Headley, and B. J. Eggleton, *Opt. Lett.* **27**, 1592 (2002).
6. T. P. White, B. T. Kuhlmeier, R. C. McPhedran, D. Maystre, G. Renversez, C. M. de Sterke, and L. C. Botten, *J. Opt. Soc. Am. B* **19**, 2322 (2002).
7. B. T. Kuhlmeier, T. P. White, G. Renversez, D. Maystre, L. C. Botten, C. M. de Sterke, and R. C. McPhedran, *J. Opt. Soc. Am. B* **19**, 2331 (2002).
8. T. P. White, R. C. McPhedran, C. M. de Sterke, L. C. Botten, and M. J. Steel, *Opt. Lett.* **26**, 488 (2001).
9. H. C. van de Hulst, *Light Scattering by Small Particles* (Wiley, New York, 1957), pp. 297–328.
10. A. C. Lind and J. M. Greenberg, *J. Appl. Phys.* **37**, 3195 (1966).